An *in vitro* vascular chip using 3D printing-enabled hydrogel casting

Biofabrication

PAPER

An *in vitro* vascular chip using 3D printing-enabled hydrogel casting

RECEIVED
28 May 2016

REVISED
27 July 2016

ACCEPTED FOR PUBLICATION
28 July 2016

PUBLISHED
26 August 2016

Liang Yang, Shivkumar Vishnempet Shridhar, Melissa Gerwitz and Pranav Soman

Department of Biomedical and Chemical Engineering, Syracuse University, 900 S Crouse Ave, Syracuse NY 13210, USA

E-mail: psoman@syr.edu

Keywords: hydrogel, microfluidic, gelatin methacrylate, encapsulation, 3D printing

Absract

An important unsolved challenge in tissue engineering has been the inability to replicate the geometry and function of vascular networks and blood vessels. Here, we engineer a user-defined 3D microfluidic vascular channel using 3D printing-enabled hydrogel casting. First, a hollow L-shaped channel is developed using a template casting process. In this process, murine 10T1/2 cells are encapsulated within gelatin methacrylate (GelMA) hydrogel using UV photocrosslinking, and upon removal of the template results in a hollow channel within GelMA. Second, human umbilical vein endothelial cells (HUVECs) were cultured within the channel and immunostaining was used to visualize endothelial monolayers. Third, diffusion/permeability studies on endothelialized channels were carried out to demonstrate the barrier function of HUVEC monolayer. Taken together, we develop a facile, cytocompatible and rapid approach to engineer a user-defined multicellular vascular chip that could be potentially useful in developing new vascular model systems.

1. Introduction

The field of tissue engineering aims to recreate a functional organ to replace or repair pathological tissues as well as serve as organ analogs for pharmacology/toxicology and disease modeling applications [1–3]. A major challenge to developing functional tissues analogs is the inability to fabricate biomimetic vasculature that can supply the essential nutrients to cells within the constructs. [4] For example, *in vivo* features such as multi-scaled branched vasculature and associated mass transport which provides the necessary exchange of oxygen, nutrients, and waste products to maintain tissue viability, cannot be accurately recapitulated using current *in vitro* systems. [5–7] As a result, new strategies which would emulate *in vivo* systems, continue to be developed.

Mimicking complex geometry has been challenging due to a limited number of manufacturing processes which can be used in the presence of living cells. A promising strategy to develop vascular network is to create channels within cell-laden hydrogel such that the channels could efficiently delivery nutrients to encapsulated cells. Hydrogels that form 3D crosslinked hydrated fibers have emerged as the ideal matrix for encapsulation of cells because of similarities to the natural extracellular matrix, as well as the ability to tune physical and biochemical properties. However, developing complex vascular geometries within cell-laden hydrogels add a significant complexity to the fabrication process as, both the time of fabrication and hydrogel properties need to be sufficiently compatible with cellular viability.

Microfabrication techniques such as soft- and photo-lithography [8–14], laser ablation, as well as newer bioprinting has enabled printing of hollow channels within cell-laden hydrogels [15–22]. Additive microfabrication techniques such as soft- and photo-lithography [8–14], as well as stacking and bonding of prefabricated hydrogels slabs have been widely adopted to fabricate microfluidic channels within cell-laden hydrogels [8–14, 23–26]. A variation of stereolithography called two-photon polymerization utilizes ultrafast lasers to crosslink hydrogels at micrometer resolution, however small working distances are typically required for this method [27]. New advances in bioprinting has enabled a hybrid additive–subtractive method for the printing of hollow channels within cell-laden hydrogels [15–22]. However most of these approaches are limited by complicated processes, and typically cannot be readily perfused. In contrast, one of the simplest methods of forming microfluidic channels is the removal of needle [28–31] from a pre-casted hydrogel. In this approach, hydrogel

precursor is poured over a metal wire/rod or glass capillary, following by removal of the template resulting in the fabrication of a lumen of uniform size. The inability of this method to fabricate branched channels has recently led to the use of sacrificial templates. However, sacrificial templates generated for perfusable channels usually involve cytotoxic organic solvents, high temperature or pressure for removing the templates, and could result in lower cellular viability [32, 33]. To avoid issues with cytotoxic chemicals releases from sacrificial templates, researchers have used biocompatible gelatin and alginate as a sacrificial element [34, 35]. New methods of producing user-defined perfusable channels in the presence of living cells continue to be developed.

In this work, multicellular vascular channels are developed using a 3D printed template within gelatin methacrylate (GelMA) hydrogel construct. 3D printing offers a method to fabricate complex geometries facilitating precise control over geometry-induced flow changes. This approach was used to form a two-cellular channel with murine 10T1/2 encapsulated within the GelMA matrix while human endothelial cells lining the lumen surface. Formation of confluent monolayers of endothelial cells within the fabricated channels was demonstrated using permeability experiments with fluorescently labeled molecules. Overall, this work demonstrates a robust, inexpensive, and biocompatible method to develop a vascular model with user-defined geometry.

2. Experimental

2.1. GelMA preparation

GelMA macromer was synthesized using a previously reported protocol [29]. Briefly, 10 g porcine skin gelatin (Sigma Aldrich, St. Louis, MO) was mixed in 200 ml phosphate buffered saline (PBS, Thermo Fisher Scientific), stirred at 60 °C, and methacrylic anhydride was added to the solution and stirred for another 3 h. To remove the unreacted groups from the solution, the mixture was dialyzed against distilled water for 1 week at 40 °C, lyophilized for 1 week. To prepare 10% (w/v) GelMA, a stock solution was prepared by mixing 1 g freeze dried GelMA with PBS (dissolved at 40 °C) with 10 ml of PBS (dissolved at 40 °C) and 0.1% UV photoinitiator Irgacure 2959 (Specialty Chemicals, Basel, Switzerland). The stock solution was sterile filtered and stored at room temperature in autoclaved Pyrex bottles (Corning). Based on the density of methacrylate = 1.035 g ml^{-1}, the molecular weight of GelMA macromer was calculated to ~590 Da. The GelMA solution was stored in a tube fully wrapped with aluminum foil, and was used about 2 h after preparation.

2.2. Fabrication of GelMA microfluidic chip

The general strategy was to use 3D printed polylactic acid (PLA) as a sacrificial template in order to create a hollow channel within GelMA matrix. First, a commercial printer (Makerbot) was used to print an L-shape PLA mold (figure 1(A)) (square cross-section area ~4 mm^2) using optimized printing parameters (100% infill; layer thickness = 0.1 mm; extruder temperature = 230 °C, extrusion speed = 75 mm s^{-1}). Polydimethysiloxane (PDMS) was prepared (10:1 ratio of silicon base Sylgard to curing agent) and poured onto the L-shape PLA mold, and cured at 65 °C on a hot plate for 2.5 h, to fabricate a reverse replica mold (figures 1(B) and (C)). To fabricate the top insert, a smaller L-shaped PLA mold (square cross-section area ~0.25 mm^2 figure 1(A)) was printed and placed inside the PDMS mold. Liquid 15% GelMA at 37 °C was poured within the gaps between the PDMS and PLA mold, and was allowed to gel at room temperature. Post gelation, PLA sacrificial mold was removed leaving behind a hollow channel open from three sides (figures 1(D) and (E)). The bottom GelMA insert is fabricated within PDMS mold in a similar manner, however in this case a sacrificial PLA mold is not used (figure 1(F)). The final assembly involves joining the PDMS inserts together and exposing both the top and bottom sides of the chip with UV light (figure 1(G)). UV exposure (Omnicure S2000, 365 nm wavelength, 150 s) results in GelMA crosslinking thereby sealing the top and bottom GelMA inserts. For cell-encapsulation experiments, 15% GelMA was mixed with 10T1/2 cells at 37 °C, with all other steps being the same. It is worth nothing that GelMA is in liquid state at 37 °C, and in a semi-solid gel state at room temperature.

2.3. Cell culture and characterization

Human umbilical vein endothelial cells (HUVECs) (Life Technologies) at passage numbers 3–8 and C3H/10T1/2 murine mesenchymal progenitor cells (10T1/2s) before passage number 15 were used. Both HUVECs and 10T1/2s cell lines were cultured in media consisting of EBM-2 (Lonza) supplemented with endothelial growth bullet-kit of EGM-2 (Lonza), and basal medium eagle (Thermo Fisher Scientific) supplemented with 10% fetal bovine serum (FBS), 1% Glutamax, and 1% Penstrap respectively, in 37 °C incubator with 5% CO_2 and ambient oxygen.

Prior to encapsulation, 10T1/2s were mixed with 15% GelMA pre-polymer solution at a density of 5×10^5 cells ml^{-1}. The GelMA-cell solution was injected into the mold as described in section 2.2, allowed to undergo gelation at room temperature, before removing the PLA template. After formation of a closed GelMA chip with encapsulated 10T1/2s, media was infused into the lumen, and changed 2 times a day. Next, HUVECs were trypsinized and suspended in the media with density of 30×10^6 cells ml^{-1}, and introduced into the GelMA

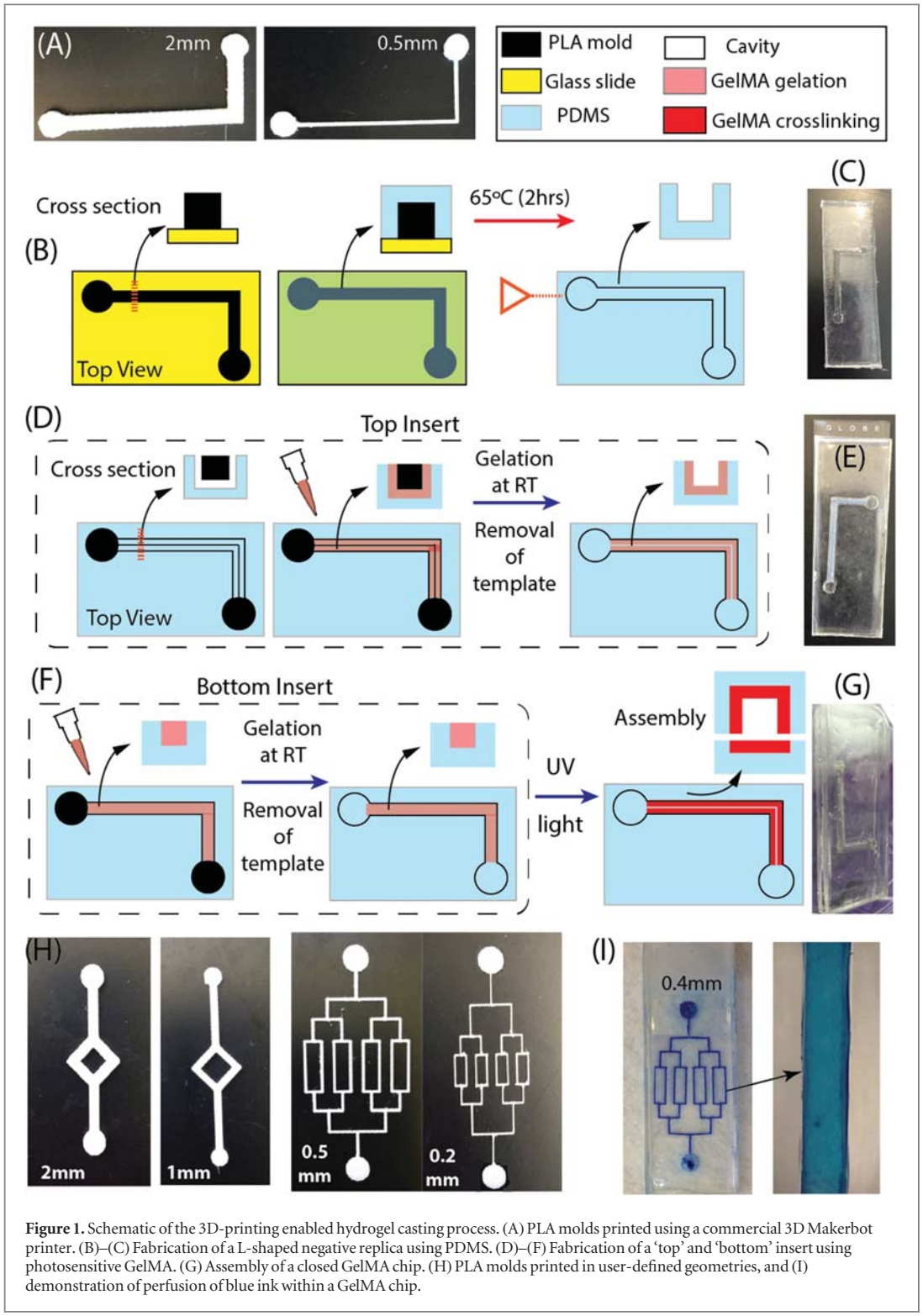

Figure 1. Schematic of the 3D-printing enabled hydrogel casting process. (A) PLA molds printed using a commercial 3D Makerbot printer. (B)–(C) Fabrication of a L-shaped negative replica using PDMS. (D)–(F) Fabrication of a 'top' and 'bottom' insert using photosensitive GelMA. (G) Assembly of a closed GelMA chip. (H) PLA molds printed in user-defined geometries, and (I) demonstration of perfusion of blue ink within a GelMA chip.

lumen via a syringe pump (NE-300 Just Infusion Syringe pump). During this experiment, HUVECs were allowed to adhere to the GelMA surface for about 4–6 h, before washing out the non-adhered cells. After the washing step, connecting tubes were used to continuously perfuse media at flow rate of 4.5×10^{-4} m s^{-1} (0.95 μl min^{-1}) for about 7 days. Chips were placed within a humidified incubator at 37 °C and 5% CO_2. Control experiments with static culture were also performed. In these experiments, HUVEC monolayer was formed on pure GelMA and GelMA + 10T1/2s in the absence of media perfusion.

Viability of 10T1/2s were determined using a Live/Dead assay Kit (Invitrogen). After 5 and 12 days

of culture, cells were fixed *in situ* with 3.7% paraformaldehyde (Invitrogen, Carlsbad, CA), washed three times with PBS, and stained for platelet endothelial cell adhesion molecule-1 (PECAM), VE-cadherin, f-actin and nucleus. For HUVECs, the device were first incubated for 30 min at room temperature in a blocking solution consisting of 10% FBS and 0.2% Triton-X, with subsequent incubation in primary and secondary antibodies for 1 h. For PECAM and VE-cadherin, a mouse monoclonal antibody CD31, and a rabbit polyclonal CD144, Cadherin 5, type 2 (life technologies), diluted into blocking solution at a ratio of 1:50 was used. The f-actin staining was performed by a secondary antibody Alexa 488 (Invitrogen, Carlsbad, CA). Hoechst 33342 were used for nuclei staining. For closed chips, all reagents were infused through the microfluidic channels. Samples were imaged using a confocal microscope (Zeiss LSM 710) and analyzed using ImageJ.

2.4. Measurement of permeability

The measurements of permeability were performed using small and large molecules by infusing solution of FITC dextran (MW = 389.98 Da) and Alexa Fluor 568 (MW = 10 kDa) (Sigma-Aldrich) at a concentration of 10 μmol l^{-1} in PBS, within GelMA chips, in the presence and absence of cells. Images were captured at intervals of 5 min for a total of 20 min for FITC dextran and for a total of 40 min for Alexa Fluor using a fluorescence microscope (Leica). The change of fluorescence intensity at different times were plotted against time and then further analyzed using MATLAB software. The permeability was determined by a previously used method [5, 6]. Briefly, the radial diffusivity (*XY* direction) of FITC Dextran and Alexa Fluor within the closed GelMA was calculated by analyzing the fluorescence intensity variations along the channel (*Y*-direction). The intensity was averaged along *Z*-direction

$$\bar{I}(y, t) \equiv \frac{1}{L}\int_0^L I(y, z, t)\,\mathrm{d}z.$$

From the given assumptions and conditions, we have

$$\frac{\partial \bar{I}}{\partial t} = D\frac{\partial^2 \bar{I}}{\partial y^2} \text{ with an instantaneous source}$$

$$S(y) = \begin{cases} \bar{I}\mathrm{o}(y) & t = 0 \\ 0 & t > 0 \end{cases}.$$

Green's transient 1D solution of an instantaneous point source was used to obtain a solution for the above equation. After integration for a continuous source and applying convolution method to the equation, we obtain a real solution for the above equation.

The Fourier transform of $\bar{I}(y, t)$ yields $\hat{I}(k, t)$

After the convolution was applied, the equation were solved and simplified to get the solution, $\hat{I}(k, t) = \hat{S}(k)\mathrm{e}^{-k^2Dt}$. After this, a characteristic spatial frequency, k_0 can be defined as $k_0 \equiv \frac{2\pi}{\lambda c}$ (where λc is the inter-channel distance).

Therefore, at $k = k_0$ the same solution becomes, $\hat{I}(k_0, t) = \hat{S}(k_0)\mathrm{e}^{-k_0{}^2Dt}$. Since this equation involves complex values, the modulus (absolute values) can be taken on both sides of the equation and further simplified by taking natural logarithm (logarithm to the base e) on both sides to get

$$\ln[\mathrm{Abs}[\hat{I}(k_0, t)]] = \ln[\sqrt{(\mathrm{Re}[\hat{S}(k_0)])^2 + (\mathrm{Im}[\hat{S}(k_0)])^2}] - k_0{}^2Dt.$$

Using the above final solution, a plot of time versus the Fourier transformed peak at the characteristic spatial frequency (k_0) yielded the diffusivity (D). $D = \frac{|\mathrm{slope}|}{|k_0{}^2|}$

The time-constant (the negative of the slope) for the decay was used to calculate the diffusivity or permeability of FITC Dextran and Alexa Fluor within closed GelMA chips with and without HUVEC layer.

2.5. Shear stress simulation and numerical calculation

The shear stress in the channel of the microfluidic device was simulated using COMSOL Multiphysics software (Version 5.1.0.136 Burlington, MA). The fluid flowing through the channel was assumed to be laminar, with a no-slip boundary conditions for the inner walls and fluid velocity (0.000 45 m s^{-1}) values as obtained from experiments. The simulated model displayed shear stresses at the various regions in the inner walls of the microfluidic channel. The shear stress values obtained from the COMSOL simulation was verified from the equation $t = 6\,Q\mu/wh^2$ where Q is the volumetric flow rate which is 1.125×10^{-10} m^3 s^{-1}, μ is the viscosity of the media (1 Pa s^{-1}), w and h are the width and heights of the channel respectively (0.5 mm in this case).

3. Results and discussion

In this work, we use 3D printing-based hydrogel casting strategy to demonstrate a proof-of-concept of a multicellular vascular model fabricated in a user-defined geometry.

3.1. Fabrication of hydrogel microfluidic chip

In this work, the facile development of cell-laden vascular channels in user-defined geometries is reported. In the proposed strategy, a commercial 3D printer was used to print a template in PLA with subsequent casting of GelMA precursor and photopolymerization, and removal of PLA template (figure 1). GelMA is ideal for this work as gelatin is a denatured derivative of the most abundant protein found in the body, collagen, and has integrin cell-binding motifs for Arg–Gly–Asp (RGD). Moreover,

GelMA has semi-transparent optical properties that allow crosslinking via UV light exposure and therefore has been extensively used for cellular encapsulation studies. A concentration of 15% GelMA was found to be ideal to produce a robust cell-laden construct with necessary mechanical stiffness. The fabrication challenges included the ability to develop a replica of PLA printed template within master silicone (PDMS) mold, as well as the ability to reliably peel-off the second PLA template. This two-step template removal is necessary to conserve GelMA, especially when GelMA is laden with living cells. This conservation of cell-laden GelMA allows the use of high-concentration of cells within the construct. Also, the PDMS mold allows the integration of GelMA chip with an inlet and outlet port using conventional tubing, to facilitate media perfusion.

The PLA removal used in this work has a unique advantage over dissolution-based removal of sacrificial template utilized in previous work [32, 33]. For example, cytotoxic reaction byproducts, often associated with sacrificial templates such as carbohydrate glass coated with poly(D-lactide-co-glycolide) or Pluronic F127, are not used in this work. Use of 10%–15% GelMA prepolymer was found to not adhere to the PLA template and allows easy removal post-crosslinking. For softer GelMA (7%), delaminating of crosslinked GelMA was often observed during the PLA template removal process. Using this process, a lumen size in the range of 200–500 μm with wall thickness of 500 μm is possible with user-defined geometries (figures (H)–(I)). The design of this device includes PDMS top and bottom inserts for mechanical stability and portability. This approach is inexpensive and scalable, are only limited by the resolution of the sacrificial template. We examined the bonding of the top and bottom inserts by introducing a blue dye mixed with DI water via a syringe pump. No leakage of a blue dye was observed between the top and bottom inserts. Figures 1(H) and (I) demonstrate that user-defined microfluidic networks inside GelMA can be successfully casted.

3.2. Cellular characterization within the GelMA chip

Herein, we demonstrate the effectiveness of the proposed strategy to fabricate a hydrogel-based vascular microfluidic device with encapsulated 10T1/2 cells and a confluent monolayer of endothelial cells. The cell line 10T1/2 is a murine embryonic mesenchymal progenitor cell line, and has been shown to act as mural cells when they are co-cultured with HUVECs. Previous studies have shown that once 10T1/2s make contact with HUVECs, HUVECs actively recruit and differentiate 10T1/2s towards a smooth muscle cell lineage, which stabilize the newly formed vessel [36, 37].

First, open chips with developed with encapsulated 10T1/2s cells, and demonstrated high cellular viability on day 5 and day 12 (figure 2(A)). Cell viability 5 days after encapsulation was quantified using a Live/Dead Viability kit (Invitrogen). Calcein-AM (green) indicates intracellular esterase activity while ethidium homodimer-1 (red) indicates loss of plasma membrane integrity. F-actin labeling on Day 12 show high cellular spreading. HUVECs seeded on the open GelMA chip demonstrated adhesion and spreading of HUVECs in the presence and absence of encapsulated 10T1/2s, however in presence of encapsulated 10T1/2s, HUVEC readily form monolayer spreading across the entire GelMA surface, while in the absence of 10T1/2s, HUVECs tend to cluster into selective areas or patches (figure 2(B)). Other studies have also demonstrated robust microvascular formation in a HUVEC-10T1/2 co-culture cellular system [38].

A closed GelMA chip with encapsulated 10T1/2s was constructed as explained in section 2.2, and HUVECs were introduced into the chip on day 12 (figure 2(C)). Perfusion of media was continued for 5 days before immunostaining HUVECs for PECAM (CD31) and VE-cadherin (CD144). HUVECs form a monolayer within the lumen and demonstrate tight cell junctions and express a conventional cobble-stone configuration throughout the whole network with no detectable differences at corners. VE-cadherin staining at the intercellular junctions indicate the maintenance of the endothelial phenotype, similar to the restrictive barrier function of *in vivo* endothelium. We also investigated the influence of HUVEC monolayer on the viability of encapsulated 10T1/2 cells in a closed GelMA chip. We found that the encapsulated 10T1/2 remain 100% viable for about 0.5 mm from the lumen surface, beyond this distance dead cells can be observed (refer to [1, 2] in figure 2(D)). The flow rate of EGM-2 media was kept at 4.5×10^{-4} m s^{-1} (0.95 μl min^{-1}) with a calculated shear stress of 54 dyne cm^{-2}. Considering the high flow rate, and resulting high shear stress used in this work, the lumen seem to withstand substantial luminal pressures. The L-shaped geometry however will result in areas of high and low shear stresses, as indicated by the COMSOL simulation (figure 2(E)). Images captured from various locations along the L-shaped channels, indicate that the flow rate used in this experiment did not induce any cellular detachment. We also did not find substantial swelling of 15% GelMA within the PDMS mold, and found this fabrication assembly process to be robust and repeatable.

3.3. Permeability/diffusivity of closed GelMA chips

The endothelial monolayer lining the GelMA channels present a barrier to the transfer of nutrients from the lumen into the GelMA matrix. To test the barrier function of the chip, injection of dextran dyes with varying molecular weights (Fluorescein; Mw 398.98D and Alexa Fluor 568; Mw 10 kDa) were injected into cellular and acellular GelMA chips to test the barrier

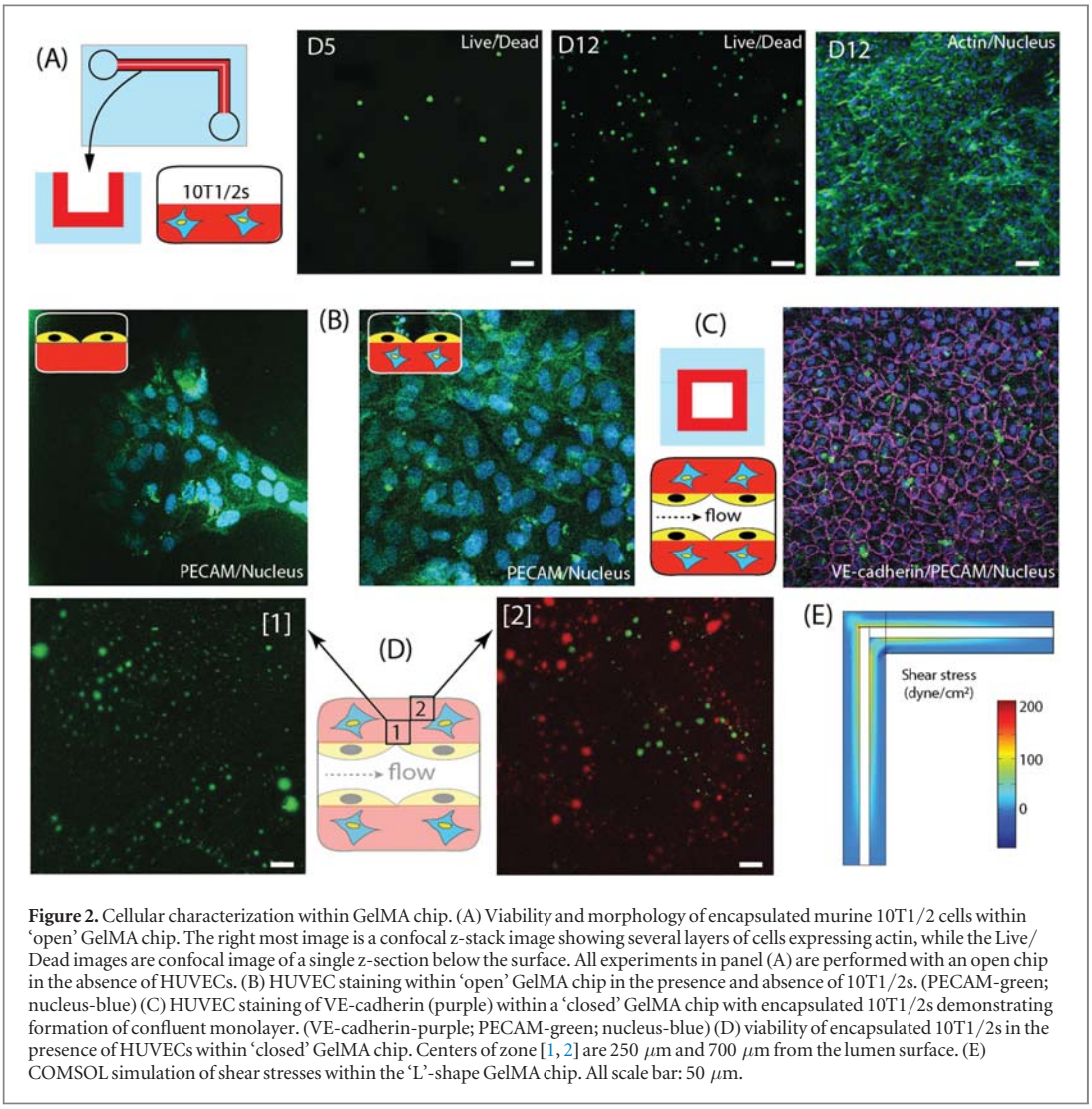

Figure 2. Cellular characterization within GelMA chip. (A) Viability and morphology of encapsulated murine 10T1/2 cells within 'open' GelMA chip. The right most image is a confocal z-stack image showing several layers of cells expressing actin, while the Live/Dead images are confocal image of a single z-section below the surface. All experiments in panel (A) are performed with an open chip in the absence of HUVECs. (B) HUVEC staining within 'open' GelMA chip in the presence and absence of 10T1/2s. (PECAM-green; nucleus-blue) (C) HUVEC staining of VE-cadherin (purple) within a 'closed' GelMA chip with encapsulated 10T1/2s demonstrating formation of confluent monolayer. (VE-cadherin-purple; PECAM-green; nucleus-blue) (D) viability of encapsulated 10T1/2s in the presence of HUVECs within 'closed' GelMA chip. Centers of zone [1, 2] are 250 μm and 700 μm from the lumen surface. (E) COMSOL simulation of shear stresses within the 'L'-shape GelMA chip. All scale bar: 50 μm.

function of the HUVEC monolayer (figure 3(A)). For this set of experiments, cellular closed-chips were created by flowing in HUVECs within 10T1/2 encapsulated GelMA on day 5. FITC dextran (green) and Alexa Fluor (red) is observed to diffusion or permeate outside the channel within the GelMA matrix. (dotted line indicates the channel edge). The fluorescence intensity plotted as a function of distance from the channel center. GelMA channels without cells show a broadening of intensity values (green plot in 3(B)) and indicates a higher diffusion rate (D) within GelMA matrix, with the slope of line plot decreasing over time (figure 3(C)), indicating a temporal diffusion from the channel into GelMA matrix. The chip lined with HUVECs show lesser broadening of the intensity thus demonstrating less permeability/leakage across the HUVEC monolayer. The higher molecular weight Alexa Fluor takes a much longer time to diffuse through the monolayer (~40 min), as compared to FITC dextran (~20 min), however both the molecules demonstrate good barrier function of the HUVEC monolayer in closed GelMA chips. The diffusivities observed from the images were calculated from the method explained in section 2.4. Briefly, Fourier transform of the Intensity values corresponding to images taken at specific time points was used to plot a best-fit linear curve to obtain the time-constant (the negative of the slope = 52 724). In this work, the dimension of the channel was 500 μm, and this value was taken as half the inter-channel distance for the calculation in this case (λc), and the spatial frequency (k_0) was determined from the equation ($k_0 = 2\pi/\lambda c = 3.140$). Using the equation $D = \frac{|\text{slope}|}{|k_0{}^2|}$, diffusivity of fluorescein and Alexa Fluor within acellular and cellular close chips were calculated. For chips with no cells, $D_{\text{flourescein}} = 1.205 \times 10^{-4}\,\text{mm}^2\,\text{s}^{-1}$, and $D_{\text{Alexa Fluor}} = 2.746 \times 10^{-5}\,\text{mm}^2\,\text{s}^{-1}$ while chips lined with HUVECs, the diffusivity was, $D_{\text{flourscein}} = 4.0647 \times 10^{-5}\,\text{mm}^2\,\text{s}^{-1}$ and $D_{\text{Alexa Fluor}} = 1.7393 \times 10^{-6}\,\text{mm}^2\,\text{s}^{-1}$. As expected, diffusivity is highest for smaller molecular weight molecule within chips with no HUVEC monolayer.

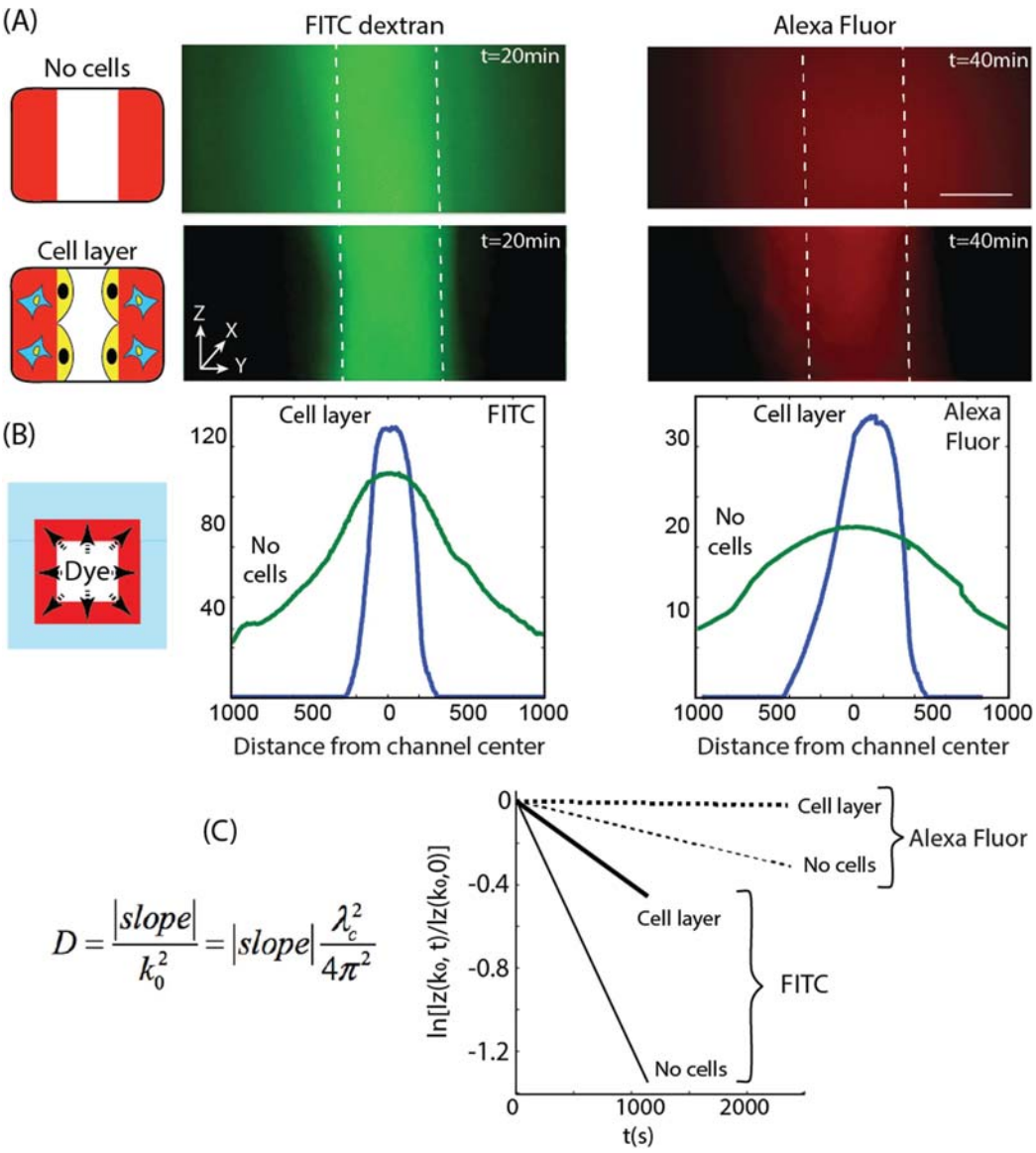

Figure 3. Permeability/diffusivity analysis within 'closed' GelMA chip. (A) Schematic and fluorescence images for FITC dextran and Alexa Fluor at specific time points with and without HUVEC lining (scale = 0.5 mm). (B)–(C) Line and logarithmic plots of change of fluorescence intensity as a function of radial distance from the center of the channel (dotted line).

Diffusional permeability was calculated based on the changing of fluorescent intensity within the GelMA channel, however this calculation is a combined effect of the permeability of molecule movement within the GelMA matrix as well as the filtration across the endothelial barriers. However, we demonstrate the differences between overall diffusional permeability between GelMA chip with and without cells. Diffusion results also support the decrease in 10T1/2 viability observed in closed chips lines with HUVECs. With GelMA chip lined with HUVECs, cell viability is high only about 0.5 mm from the lumen (figure 2(D)), however the viability decrease drastically, as we move away from the lumen, most probably due to an increase in oxygen and nutrient consumption by encapsulated cells.

The use of commercial 3D printers to develop vascular 3D models would allow researchers with non-manufacturing backgrounds to readily utilize them to investigate physiological and diseased vascular structures. The control over channel geometries, flow rates and cellular types in this work, offer a unique opportunity to develop *in vitro* models for vascular pathologies. With improved resolutions in 3D printing technology, micrometer resolution arterioles, venules and capillaries could be potentially developed. For example, the role of geometry-induced flow rates on (a) endothelial function and atherosclerotic plaque formation, (b) highly-branched blood vessels in cerebral cortex to enhance delivery of oxygen and (c) tortuous vessel geometry in glomeruli of kidney to assist

in filtration, could be investigated using such models. A limitation of this method is its inability to make capillary-sized channels, as the lumen size is limited to about 200 μm. Also this method is limited to planar 2.5D networks, and lacks the versatility of other methodologies such as stereolithography or 3D extrusion-based bioprinting.

Although PDMS-based microfluidics have made significant progress in developing physiologically relevant models for the vascular system, PDMS material and surface properties do not represent native ECM properties. As a result, hydrogel-based microfluidics are gaining interest to reproduce many of the important biochemical and biophysical characteristics of the basement membrane and interstitial matrix. Typically, needle-casting approach is used to fabricate a straight microfluidic channels which is not similar to the complex tortuous channels found in *in vivo* vasculature. Moreover, multicellular interactions and associated signals are necessary to establish *in vivo* function. To address some these deficiencies in current *in vitro* systems, we present a new hydrogel based chip with versatile control over the geometry, cellular composition and dynamic flow properties. The template-based subtractive methodology presented here, can be extended to a variety of photo-sensitive hydrogels, relevant cellular types, and networks with complex geometries. Further research in this area would enable researchers to ask new biological questions not possible with conventional platforms. For example, the influence of geometry induced effects, such as fluid transport, permeability, shear stresses on the stability of the vessels and its interactions with other cell types and biomolecules in physiological and diseased conditions could be investigated, thereby increasing fundamental understanding of vascular biology [29, 39, 40].

4. Conclusion

To address the challenge of vascularization, we developed a 3D printer-based methodology to fabricate a multi-cell vascular microfluidic chip using cell-laden GelMA. The chip exhibits a confluent endothelium lining along with close justaposition of 10T1/2 cells with sufficient cell viability. Diffusion results demonstrates that GelMA chip lined with HUVECs provides good barrier function, as characterized by permeability of fluorescence molecules. This work demonstrates an effective strategy to fabricate a hydrogel-based vascular microfluidic devices in user-defined geometries, and will potentially serve as a unique experimental tool for investigating fundamental mechanisms of vascular remodeling with extracellular matrix and maturation process under 3D flow condition, and will provide opportunities for developmental biologist and tissue engineers to test previously untested hypothesis in an *in vitro* platform.

Acknowledgments

Thanks to Professor Abraham Stroock (Department of Chemical and Biomolecular Engineering, Cornell University) and Dr Nakwon Choi (Korean Institute of Science and Technology) for being supportive and generously providing necessary materials for the permeability calculations. PS conceived the project. LY, and PS designed the experiments. SVS performed diffusion calculation and COMSOL analysis. MG synthesized GelMA hydrogel. All authors contributed to writing the paper.

References

[1] Guillemot F, Mironov V and Nakamura M 2010 Bioprinting is coming of age: report from the international conference on bioprinting and biofabrication in bordeaux (3B'09) *Biofabrication* **2** 010201
[2] Mironov V, Reis N and Derby B 2006 Review: bioprinting: a beginning *Tissue Eng.* **12** 631–4
[3] Mironov V, Boland T, Trusk T, Forgacs G and Markwald R R 2003 Organ printing: computer-aided jet-based 3D tissue engineering *Trends Biotechnol.* **21** 157–61
[4] Ozbolat I T and Yu Y 2013 Bioprinting toward organ fabrication: challenges and future trends *IEEE Trans. Biomed. Eng.* **60** 691–9
[5] Bae H *et al* 2012 Building vascular networks *Sci. Trans. Med.* **4** 160ps123
[6] Kaully T, Kaufman-Francis K, Lesman A and Levenberg S 2009 Vascularization—the conduit to viable engineered tissues *Tissue Eng.* B **15** 159–69
[7] Rouwkema J, Rivron N C and van Blitterswijk C A 2008 Vascularization in tissue engineering *Trends Biotechnol.* **26** 434–41
[8] Zheng Y *et al* 2011 Microstructured templates for directed growth and vascularization of soft tissue *in vivo Biomaterials* **32** 5391–401
[9] Nazhat S N *et al* 2007 Controlled microchannelling in dense collagen scaffolds by soluble phosphate glass fibers *Biomacromolecules* **8** 543–51
[10] Kim D-N, Lee W and Koh W-G 2008 Micropatterning of proteins on the surface of three-dimensional poly (ethylene glycol) hydrogel microstructures *Anal. Chim. Acta* **609** 59–65
[11] Ling Y *et al* 2007 A cell-laden microfluidic hydrogel *Lab Chip* **7** 756–62
[12] Cuchiara M P, Allen A C, Chen T M, Miller J S and West J L 2010 Multilayer microfluidic PEGDA hydrogels *Biomaterials* **31** 5491–7
[13] Golden A P and Tien J 2007 Fabrication of microfluidic hydrogels using molded gelatin as a sacrificial element *Lab Chip* **7** 720–5
[14] Chan V, Zorlutuna P, Jeong J H, Kong H and Bashir R 2010 Three-dimensional photopatterning of hydrogels using stereolithography for long-term cell encapsulation *Lab Chip* **10** 2062–70
[15] Skardal A, Zhang J and Prestwich G D 2010 Bioprinting vessel-like constructs using hyaluronan hydrogels crosslinked with tetrahedral polyethylene glycol tetracrylates *Biomaterials* **31** 6173–81
[16] Roth E A *et al* 2004 Inkjet printing for high-throughput cell patterning *Biomaterials* **25** 3707–15
[17] Zhao L, Lee V K, Yoo S-S, Dai G and Intes X 2012 The integration of 3D cell printing and mesoscopic fluorescence molecular tomography of vascular constructs within thick hydrogel scaffolds *Biomaterials* **33** 5325–32
[18] Zhang Y, Yu Y and Ozbolat I T 2013 Direct bioprinting of vessel-like tubular microfluidic channels *J. Nanotechnol. Eng. Med.* **4** 020902

[19] Fang Z, Starly B and Sun W 2005 Computer-aided characterization for effective mechanical properties of porous tissue scaffolds *Comput.-Aided Des.* **37** 65–72
[20] Bertassoni L E *et al* 2014 Hydrogel bioprinted microchannel networks for vascularization of tissue engineering constructs *Lab Chip* **14** 2202–11
[21] Dababneh A B and Ozbolat I T 2014 Bioprinting technology: a current state-of-the-art review *J. Manuf. Sci. Eng.* **136** 061016
[22] Yu Y, Zhang Y, Martin J A and Ozbolat I T 2013 Evaluation of cell viability and functionality in vessel-like bioprintable cell-laden tubular channels *J. Biomech. Eng.* **135** 091011
[23] Wong K H K, Chan J M, Kamm R D and Tien J 2012 Microfluidic models of vascular functions *Annu. Rev. Biomed. Eng.* **14** 205–30
[24] Price G M *et al* 2008 Bonding of macromolecular hydrogels using perturbants *J. Am. Chem. Soc.* **130** 6664–5
[25] Zheng Y *et al* 2012 *In vitro* microvessels for the study of angiogenesis and thrombosis *Proc. Natl Acad. Sci.* **109** 9342–7
[26] Sarig-Nadir O, Livnat N, Zajdman R, Shoham S and Seliktar D 2009 Laser photoablation of guidance microchannels into hydrogels directs cell growth in three dimensions *Biophys. J.* **96** 4743–52
[27] Xing J-F, Zheng M-L and Duan X-M 2015 Two-photon polymerization microfabrication of hydrogels: an advanced 3D printing technology for tissue engineering and drug delivery *Chem. Soc. Rev.* **44** 5031–9
[28] Chrobak K M, Potter D R and Tien J 2006 Formation of perfused, functional microvascular tubes *in vitro Microvascular Res.* **71** 185–96
[29] Price G M *et al* 2010 Effect of mechanical factors on the function of engineered human blood microvessels in microfluidic collagen gels *Biomaterials* **31** 6182–9
[30] Nichol J W *et al* 2010 Cell-laden microengineered gelatin methacrylate hydrogels *Biomaterials* **31** 5536–44
[31] Park J H *et al* 2010 Microporous cell-laden hydrogels for engineered tissue constructs *Biotechnol. Bioeng.* **106** 138–48
[32] Bellan L M *et al* 2012 Fabrication of a hybrid microfluidic system incorporating both lithographically patterned microchannels and a 3D fiber-formed microfluidic network *Adv. Healthcare Mater.* **1** 164–7
[33] Khattak S F, Bhatia S R and Roberts S C 2005 Pluronic F127 as a cell encapsulation material: utilization of membrane-stabilizing agents *Tissue Eng.* **11** 974–83
[34] Golden A P and Tien J 2007 Fabrication of microfluidic hydrogels using molded gelatin as a sacrificial element *Lab Chip* **7** 720–5
[35] Wang X-Y *et al* 2014 Engineering interconnected 3D vascular networks in hydrogels using molded sodium alginate lattice as the sacrificial template *Lab Chip* **14** 2709–16
[36] Hirschi K K, Rohovsky S A and D'Amore P A 1998 PDGF, TGF-β, and heterotypic cell–cell interactions mediate endothelial cell–induced recruitment of 10T1/2 cells and their differentiation to a smooth muscle fate *J. Cell Biol.* **141** 805–14
[37] Hirschi K K, Rohovsky S A, Beck L H, Smith S R and D'Amore P A 1999 Endothelial cells modulate the proliferation of mural cell precursors via platelet-derived growth factor-BB and heterotypic cell contact *Circ. Res.* **84** 298–305
[38] Cuchiara M P, Gould D J, McHale M K, Dickinson M E and West J L 2012 Integration of self-assembled microvascular networks with microfabricated PEG-based hydrogels *Adv. Funct. Mater.* **22** 4511–8
[39] Culver J C and Dickinson M E 2010 The effects of hemodynamic force on embryonic development *Microcirculation* **17** 164–78
[40] Stroock A D and Fischbach C 2010 Microfluidic culture models of tumor angiogenesis *Tissue Eng.* A **16** 2143–6